



Anomalously deep mantle transition zone below Central Europe: Evidence of lithospheric instability

György Hetényi,^{1,2,3,4} Graham W. Stuart,¹ Gregory A. Houseman,¹ Frank Horváth,³
Endre Hegedűs,⁵ and Ewald Brückl⁶

Received 23 July 2009; revised 10 September 2009; accepted 13 October 2009; published 11 November 2009.

[1] The depths of the 410 and 660 km phase transitions provide critical information on the thermal state of the mantle transition zone (MTZ) and, by implication, on the circulation of the upper mantle. We analyze converted seismic waves to produce a high resolution image of these discontinuities beneath the Pannonian Basin of Central Europe. Models to explain the extension of the basin in the Middle Miocene involve subduction roll-back and gravitational instability of an over-thickened lithosphere. We find that cold dense material appears to have accumulated in the MTZ, consistent with the idea of supply from several subduction episodes, or upper mantle overturn. Variation in depth of the 660 km discontinuity by as much as 40 km suggests that cold lithospheric mantle is ponding on top of this phase transition. Where the phase transition is deepest, eventual transfer of this material into the lower mantle may be expected to develop. **Citation:** Hetényi, G., G. W. Stuart, G. A. Houseman, F. Horváth, E. Hegedűs, and E. Brückl (2009), Anomalously deep mantle transition zone below Central Europe: Evidence of lithospheric instability, *Geophys. Res. Lett.*, *36*, L21307, doi:10.1029/2009GL040171.

1. Introduction

[2] Formation of the Pannonian Basin in the Middle Miocene occurred essentially by rapid extension of orogenic terranes during their escape from the Alpine collision zone towards the east [Horváth, 1993]. These processes are inferred to have been driven by a subduction system operating on the Eastern Carpathians [e.g., Horváth and Royden, 1981]. The relatively large ratio of mantle thinning factor to crustal thinning factor, as determined by subsidence histories in the basin, implies that gravitational instability of the lithospheric mantle [Houseman and Gemmer, 2007] was also a significant driving force. Detachment of the Pannonian lower lithosphere could have occurred either in the Alpine collision zone before escape [Horváth et al., 2005a] or during and after extension [Houseman and Gemmer, 2007]. These mechanisms require that subducted or delaminated lithosphere has descended into the upper mantle and has dis-

placed hot material which has moved upwards beneath the extending basin. Models of mantle convection imply that the effects of such an overturn should extend throughout the upper mantle, but may have had minimal impact so far on the lower mantle because the time-scale for viscous deformation of the lower mantle is so much greater than that of the upper mantle, and the extension finished only 10 Myr ago. To the first order, regional P-wave tomographic inversions beneath the Pannonian Basin [Wortel and Spakman, 2000; Piromallo and Morelli, 2003] support this model by showing that anomalously fast material occupies the mantle transition zone (MTZ), beneath anomalously slow upper mantle. The vertical extent of the fast anomaly is, however, not clear as tomographic techniques do not have sufficient resolution in depth.

[3] To quantify the extent and impact of the mantle dynamical processes described above, we examine the deflection of the major phase change interfaces bounding the MTZ by computing receiver functions (RF) from a high-resolution broad-band seismic dataset combining a recent array deployment across the Pannonian Basin and permanent stations. These phase changes are *olivine* → *wadsleyite* at ~410 km, and *ringwoodite* → *perovskite* + *magnesiowüstite* at ~660 km depth. The positive Clapeyron slope of the 410 km transition encourages vertical transport because the phase transition is elevated in cold downwelling regions, whereas the 660 km transition, with negative Clapeyron slope, is depressed in cold regions and thus resists exchange of material with the lower mantle. A thickened (thinned) mantle transition zone is usually interpreted in terms of a colder (warmer) thermal regime than the laterally averaged mantle temperatures [e.g., Lebedev et al., 2002]. In Central Europe, we discover that while the top of the MTZ is close to its expected depth (410 km), its bottom is clearly depressed below 660 km and shows significant undulations. We argue that these undulations arise from the uneven accumulation of cold material from successive episodes of subduction and/or gravitational instability of the lithospheric mantle. The depressed areas of the 660 km discontinuity beneath the Pannonian Basin indicate the places where local downwelling into the lower mantle may develop, if not already occurring.

2. Geodynamic Setting and Scenario

[4] Central Europe has been a tectonically active zone since the Cretaceous and throughout the Cenozoic. The region, lying in the eastern extension of the main collision zone between Africa and Europe, the Alps, has experienced a complex geodynamic history. At the end of the Cretaceous and during the Palaeogene, a mosaic of continental terranes

¹School of Earth and Environment, University of Leeds, Leeds, UK.

²Laboratoire de Géologie, UMR8538, Ecole Normale Supérieure, CNRS, Paris, France.

³Department of Geophysics, Eötvös University, Budapest, Hungary.

⁴Department of Earth Sciences, ETH Zurich, Zurich, Switzerland.

⁵Eötvös Loránd Geophysical Institute, Budapest, Hungary.

⁶Institute of Geodesy and Geophysics, Technische Universität Wien, Vienna, Austria.

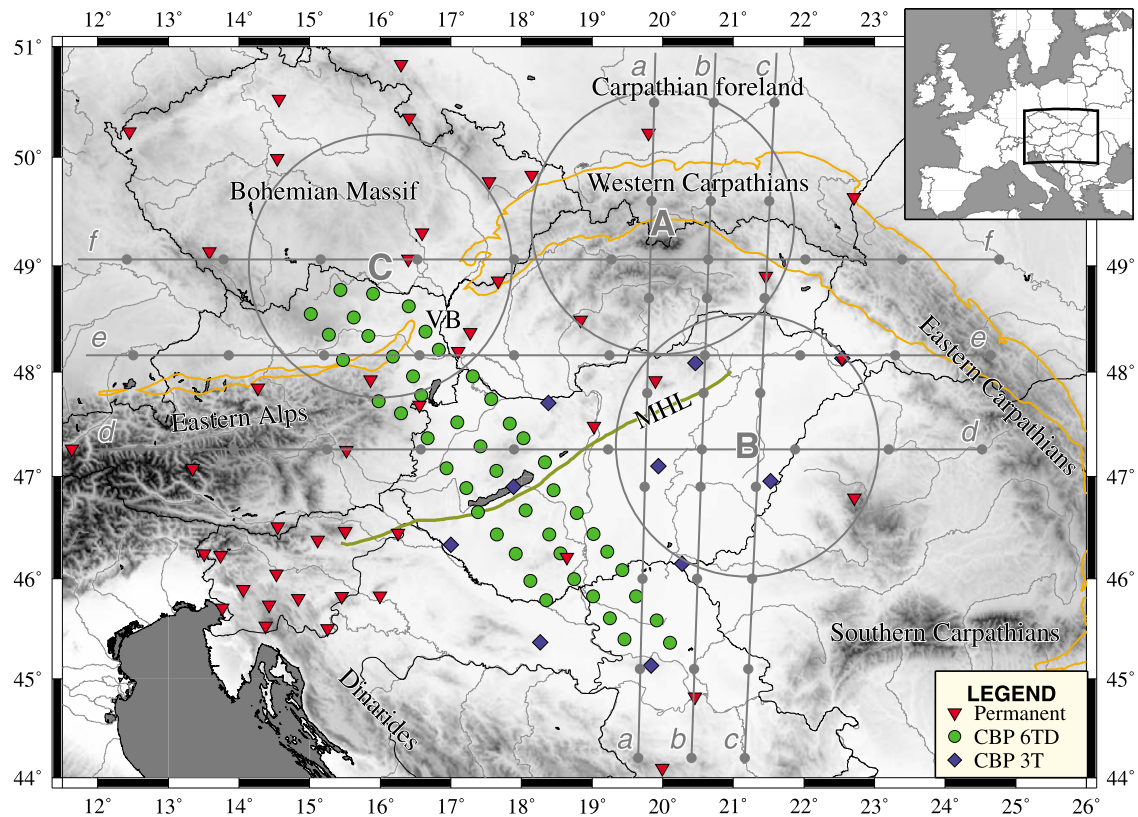


Figure 1. Study area and station location for the Carpathian Basins Project (2005–2007). The Pannonian Basin is surrounded by mountain ranges resulting from several episodes of collision and subduction between Africa and Europe. VB, Vienna pull-apart basin. MHL, Mid-Hungarian Line, dividing two micro-terranes (Alcampa to the North and Tisza to the South) in the Pannonian Basin. The orange line shows the extent of the flysch formation of the Outer Carpathians. Permanent broadband station data were accessed through GEOFON (<http://geofon.gfz-potsdam.de/geofon/>), ORFEUS (<http://www.orfeus-eu.org/>), and IRIS (<http://www.iris.edu/hq/>), as well as from the Geodetic and Geophysical Research Institute of the Hungarian Academy of Sciences. Temporary stations used Guralp 6TD and 3T instruments. Migrated profiles a-f are shown on Figure 2 with dots at 100 km intervals, circles A-C are 140 km radii areas for waveform stacking (see Figure S3).

and Neo-Tethys-related oceanic lithosphere fragments governed the evolution of this area [Csonos and Vörös, 2004; Stampfli and Borel, 2004; Schmid et al., 2008]. The successive subduction and accretion of these micro-terranes set the scene for the formation of the extensional Pannonian Basin, with deep sedimentary basins, and the rise of the surrounding mountain ranges, the Carpathians and the Dinarides (Figure 1). The latest and currently most active part in this range is the Vrancea zone, where Eastern and Southern Carpathians meet [Bada et al., 1999; Lorinczi and Houseman, 2009].

[5] Geophysical measurements in the Pannonian Basin show that the crust and the lithosphere are thinned beneath the entire basin, and that the thermal regime is warmer than the global continental average [Horváth et al., 2005b; Šroda et al., 2006; Brückl et al., 2007]. Beneath the lithosphere, the asthenosphere is thought to be hot, as indicated by magnetotelluric measurements [e.g., Adam et al., 1989] and seismic tomography [Wortel and Spakman, 2000; Piromallo and Morelli, 2003]. These latter studies also show clear (>1.5–2%) fast anomalies in the MTZ beneath all of the Pannonian Basin, which the authors interpret as remnants of

recent subduction episodes. Concerning the Vrancea region, the same tomography results show a separate sub-vertical fast anomaly, extending down to ~400 km depth.

3. Data and Processing

[6] Figure 1 shows the broad-band seismological stations providing data for our study: three profiles from the Carpathian Basins Project (CBP) operated for 16 months, and we obtained data from permanent stations over a 4-year period. We use the receiver function technique that captures P- to S-wave conversions at velocity discontinuities within the Earth [Langston, 1979]. Frequencies between 0.033 and 0.25 Hz were kept by filtering in order to detect conversions from the MTZ. The RF delay times were then converted to depth using the regional PM05 velocity-model [Piromallo and Morelli, 2003], and the conversion points (Figure S1 of the auxiliary material) migrated to their correct geometric positions [Zhu, 2000].¹ These converted signals were

¹Auxiliary materials are available in the HTML. doi:10.1029/2009GL040171.

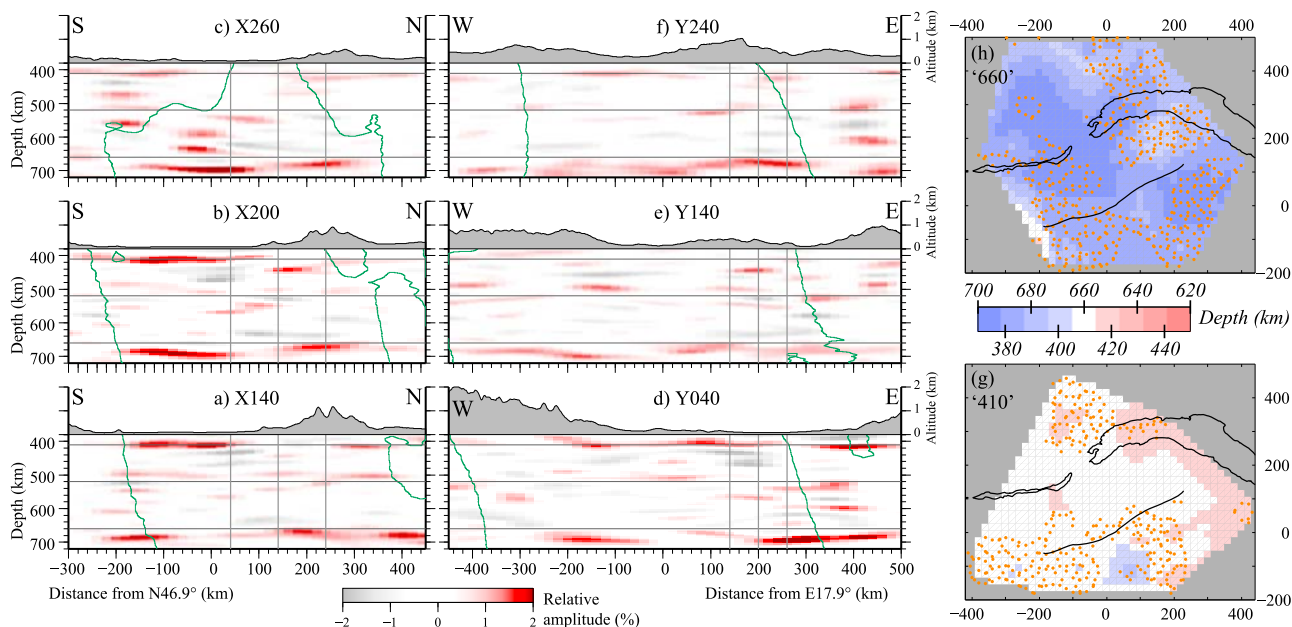


Figure 2. Mantle transition zone structure presented in profile as well as in map view. Migrated receiver function profiles of the mantle transition zone along (a–c) S–N and (d–f) W–E directions (see Figure 1 for locations, as well as the averaged topography above each profile for reference). Red colors indicate positive impedance contrast with depth. Thin horizontal lines are drawn at 410, 520 and 660 km depth. Thin vertical lines show location of intersections with perpendicular profiles. Thin green lines bound well-resolved areas of the image, i.e., with more than 20% of the maximum ray coverage (g–h). Map view of the mantle transition zone interface depth beneath the study area. First, the (g) 410 and (h) 660 km discontinuities were picked manually (orange dots) and interpolated to produce depth maps. Depths were picked only within the well resolved part of the image (i.e., more than 20% of the maximum ray coverage); the remaining part of the image is in grey. The significant thickening is caused by the deflection of the ‘660’, the ‘410’ being close to its expected depth. The Mid-Hungarian Line and the Carpathian flysch are drawn for reference.

binned into voxels and smoothed, accounting for the size of the Fresnel zone and the vertical resolution of the RF, to produce the final images of the MTZ discontinuity depths. Details of data and processing are given in the auxiliary material.

4. Results

[7] Six slices of our 3-D migrated image (see Figure 1 for locations), representative of the observed features are shown on Figures 2a–2f. Relative to the typical depth of the 410 and 660 km discontinuities (‘410’ and ‘660’ hereinafter), we can observe that:

[8] 1. The converted amplitudes associated with the ‘410’ are sub-horizontal, and lie at their normal depth, with deviations rarely exceeding 10 km.

[9] 2. On the other hand, the conversions from the ‘660’ are imaged clearly deeper than the global average, with apparent depths ranging from ~ 665 km to ~ 700 km.

[10] 3. Significantly weaker and localized conversion amplitudes are observed at or around the proposed discontinuity at 520 km depth (*wadsleyite* \rightarrow *ringwoodite* phase change).

[11] These observations imply that the mantle transition zone below the Pannonian Basin is in general thicker than the global average (250 km estimated by *Chevrot et al.* [1999]; 242 ± 2 km by *Lawrence and Shearer* [2006]) by up

to 40 km. Lateral variations in thickness can be assessed on the RF waveforms (see auxiliary material) as well as in map-view: interpolated surfaces of both the ‘410’ and the ‘660’ were obtained by manual picking on both N–S and E–W oriented slices (Figures 2g and 2h). Figures 2g and 2h demonstrate, at least in the well resolved parts (see auxiliary material) of our image, that the MTZ thickening is a result of the clear deepening of the ‘660’, while the ‘410’ shows no significant deviation.

[12] Our results broadly agree with previous investigations of the mantle transition zone beneath Central Europe based on reflected and refracted phases from regional events [*Świeczak et al.*, 2004] and on RFs from fewer stations [*Hetényi and Bus*, 2007; *Geissler et al.*, 2008], and bring a new, higher resolution, three-dimensional image of the MTZ in this region. The new images show variations in depth of the ‘660’ conversions occurring with wavelengths on the order of 200 km, forming visible undulations such as a bowl-shaped depression below the Eastern part of the Pannonian Basin (see the centre of profile *b* and *c*, as well as the Eastern part of profile *d*), which are independent from variations in V_p/V_s within the MTZ (see auxiliary material). Comparison of our results with those from a similar study of the Alps [*Lombardi et al.*, 2009] raises important questions: in both cases the ‘660’ is deeper by as much as 40 km, yet Alpine geology has been dominated by continental convergence since 15 Ma, whereas the Pannonian system underwent

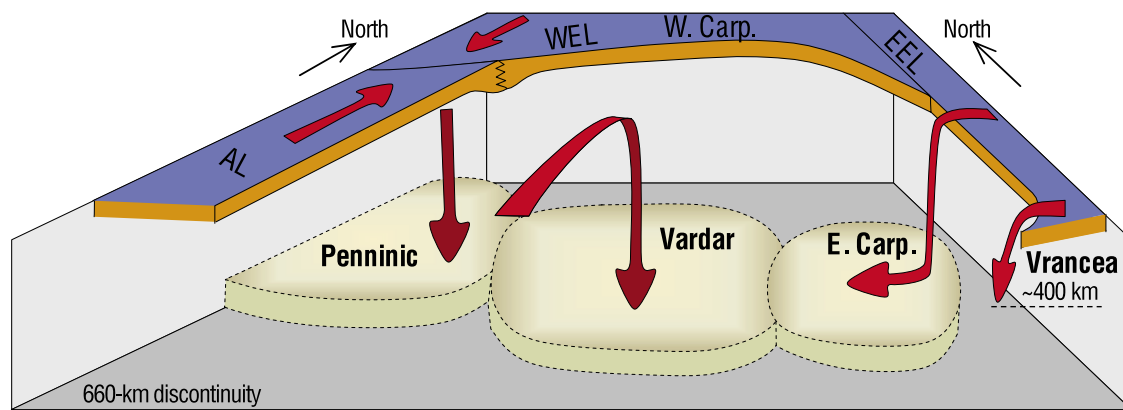


Figure 3. Schematic representation of lithospheric relationships and evolution in the Pannonian Basin region. Blue-yellow colors mark the Adriatic (AL), the West European (WEL) and the East European (EEL) lithospheres. Red arrows represent lithosphere movement paths along which lithospheric material have reached the mantle transition zone. The pale brown bodies represent the areas where the following ocean remnants have sunk: Penninic in the Cretaceous, Vardar in the Palaeogene, and the East Carpathian subduction in the Miocene. The next source of lithospheric material will be the arrival of the Vrancea zone into the mantle transition zone, currently extending down to a depth of ~ 400 km.

a phase of rapid extension followed by structural stabilization since 10 Ma. Is depression of the ‘660’ in both regions actually related to lithospheric events that occurred prior to 10 Ma or even earlier?

5. Discussion and Conclusions

[13] In the context of subduction, a thickened MTZ is usually interpreted in terms of a colder thermal regime than the ambient mantle temperatures [e.g., *Lebedev et al.*, 2002]. In order to explain a ~ 40 km MTZ thickening solely as an effect of temperature, a negative anomaly of the order of 300 K is required throughout the MTZ (considering Clapeyron-slopes of 2.9 and -1.9 MPa/K for the ‘410’ and the ‘660’, respectively [*Bina and Helffrich*, 1994]). However, our results beneath the Pannonian-Carpathian region provide complementary information with better spatial resolution than earlier tomographic images [*Wortel and Spakman*, 2000; *Piomallo and Morelli*, 2003]. Thickening is mainly caused by deepening of the ‘660’ without major variation in the depth of the ‘410’. Direct conversion of these anomalies in depth to thermal anomalies at the interfaces using the above Clapeyron-slopes would imply normal mantle temperatures at the ‘410’, and temperatures lower than normal by up to 800 K at the ‘660’.

[14] In the light of tomography and RF results, and the geodynamic history of the region, we interpret the anomalously deep 660 km transition as a result of accumulation of cold, denser material. Similar magnitude deflections of the ‘660’ are observed where subducting slabs are actively impinging on the lower mantle [*Shearer and Masters*, 1992; *Li et al.*, 2000]. Such observations beneath the NW Pacific have been interpreted as showing the downward movement of the cold upper mantle through the petrological barrier of the 660 km discontinuity [*Li and Yuan*, 2003]. Observations similar to ours of a flat ‘410’ but structurally complicated and deepened ‘660’ have been described beneath the eastern part of the North China Craton [*Chen and Ai*, 2009] and interpreted as a stagnant slab with possible sporadic penetration into the lower mantle. One

might also argue that localized depressions of the ‘660’ are caused by ponding of relatively cold lithospheric mantle material, accumulated during different subduction or continental delamination events, but not yet penetrating the phase transition boundary. Non-olivine phase transitions, such as *garnet* \rightarrow *perovskite* are also proposed to explain complex RF signature of the ‘660’ as these can generate multiple discontinuities and velocity gradients [*Andrews and Deuss*, 2008]. Close examination of our images has not found clear evidence of such broadened or duplicated signal. The simplest explanation of this absence is that this recently deposited cold material of lithospheric provenance has not undergone the phase change associated with the ‘660’.

[15] A schematic geodynamic interpretation of the provenance of subducted or delaminated lithospheric material is shown on Figure 3. Cold material in the MTZ has been accumulating since at least the Cretaceous, from sustained continental convergence and successive subduction of Neo-Tethys-related sub-basins. Associated with the collision of Africa with Europe, the Penninic oceanic fragment has sunk into the MTZ in the Cretaceous—Early Palaeogene [*Csontos and Vörös*, 2004; *Schmid et al.*, 2008]. The Vardar Ocean, whose suture lies to the southwest of the Pannonian Basin has disappeared in a second stage of convergence during the Palaeogene [*Csontos et al.*, 1992; *Kovács et al.*, 2007], as has the Ligurian oceanic fragment west of the Apennines [*Faccenna et al.*, 2004]. In the Miocene from 17 to 11 Ma the Carpathian flysch basin lithosphere has been apparently consumed by the East Carpathian subduction zone [*Horváth*, 1993]. Though subduction ceased at 11 Ma, sinking of cold, possibly continental mantle towards the MTZ continues beneath the SE Carpathians at least [*Lorinczi and Houseman*, 2009]. At present, lithospheric material of different age and provenance occupies the MTZ (Figure 3): it is unlikely that these fragments continue to behave as slabs, but rather deform viscously as they are sheared and mixed by a continuing convective circulation. This complex history may explain the irregular lateral variation in depth of the ‘660’.

[16] The fact that cold material fills the MTZ beneath the Pannonian Basin, seen now by both tomography and receiver function images from independent data, has implications for the thermal regime and volcanism of the region. The observed high heat flow at surface [Horváth *et al.*, 2005b], the slow seismic anomalies above the MTZ [Wortel and Spakman, 2000; Piromallo and Morelli, 2003], the high electrical conductivities [e.g., Ádám *et al.*, 1989], and the potential upward displacement of hot material by the sinking slabs all call for a hot upper mantle. In addition dehydration of descending slabs [Ono, 2007] may have released water into the upper mantle, which triggered post-Miocene volcanism in the Pannonian Basin [Harangi *et al.*, 2007]. Although a plume originating in the lower mantle is proposed for continental European volcanic areas [Goes *et al.*, 1999], the downward deflection of the 660 km discontinuity almost everywhere beneath the Pannonian-Carpathian region implies that this plume is unlikely to have strongly impacted the upper mantle in this region. Indeed, an upper mantle source for the observed volcanism seems more probable, which is also supported by geochemistry, tomography and plate kinematics [Piromallo *et al.*, 2008].

[17] In conclusion, the Pannonian Basin is a region with a complex geodynamical history of subduction, lithospheric deformation and gravitational instability reflected now in structures observed in the mantle transition zone. The history of subduction events and continuing lithospheric instability integrated over Cretaceous and Cenozoic times explains in principle the observed thickening of the MTZ which is now imaged here in unprecedented detail.

[18] **Acknowledgments.** The authors are grateful for the help of others in the CBP Working Group (S. Radovanovic, A. Brisbourne, A. Horleston, D. Hawthorn, P. Lorinczi, B. Dando, G. Falus, A. Kovács, I. Török, H. Hausmann, W. Loderer, V. Kovacevic, S. Petrovic-Cacic, D. Valcic), as well as to the following institutes: SEIS-UK for providing the seismological stations for the Carpathian Basins Project; GEOFON, ORFEUS and IRIS repositories for permanent station data; as well as the Geodetic and Geophysical Research Institute of the Hungarian Academy of Sciences for granting access to permanent station data in Hungary. Many thanks to Claudia Piromallo who provided immediate access to the PM05 velocity-model. The paper benefited from constructive and concise reviews from two anonyms, as well as from discussions with George Helffrich, Sebastian Rost and Marjorie Wilson. Figures 1, 2 and S1 were produced using the Generic Mapping Tool [Wessel and Smith, 1991]. The Carpathian Basins Project was funded by NERC standard grant NE/C004574/1.

References

- Ádám, A., K. Landy, and Z. Nagy (1989), New evidence for the distribution of the electric conductivity in the Earth's crust and upper mantle in the Pannonian Basin as a "hotspot," *Tectonophysics*, *164*, 361–368, doi:10.1016/0040-1951(89)90027-9.
- Andrews, J., and A. Deuss (2008), Detailed nature of the 660 km region of the mantle from global receiver function data, *J. Geophys. Res.*, *113*, B06304, doi:10.1029/2007JB005111.
- Bada, G., F. Horváth, P. Gerner, and I. Fejes (1999), Review of the present-day geodynamics of the Pannonian basin: Progress and problems, *J. Geodyn.*, *27*, 501–527, doi:10.1016/S0264-3707(98)0013-1.
- Bina, C. R., and G. Helffrich (1994), Phase transition Clapeyron slopes and transition zone seismic discontinuity topography, *J. Geophys. Res.*, *99*, 15,853–15,860, doi:10.1029/94JB00462.
- Brückl, E., *et al.* (2007), Crustal structure due to collisional and escape tectonics in the Eastern Alps region based on profiles Alp01 and Alp02 from the ALP 2 002 seismic experiment, *J. Geophys. Res.*, *112*, B06308, doi:10.1029/2006JB004687.
- Chen, L., and Y. Ai (2009), Discontinuity structure of the mantle transition zone beneath North China Craton from receiver function migration, *J. Geophys. Res.*, *114*, B06307, doi:10.1029/2008JB006221.
- Chevrot, S., L. Vinnik, and J.-P. Montagner (1999), Global-scale analysis of the mantle *Pds* phases, *J. Geophys. Res.*, *104*, 20,203–20,219, doi:10.1029/1999JB900087.
- Csontos, L., and A. Vörös (2004), Mesozoic plate tectonic reconstruction of the Carpathian region, *Palaeogeogr. Palaeoclimatol. Palaeoecol.*, *210*, 1–56, doi:10.1016/j.palaeo.2004.02.033.
- Csontos, L., A. Nagymarosy, F. Horváth, and M. Kovác (1992), Tertiary evolution of the Intra-Carpathian area: A model, *Tectonophysics*, *208*, 221–241, doi:10.1016/0040-1951(92)90346-8.
- Faccenna, C., C. Piromallo, A. Crespo-Blanc, L. Jolivet, and F. Rossetti (2004), Lateral slab deformation and the origin of the western Mediterranean arcs, *Tectonics*, *23*, TC1012, doi:10.1029/2002TC001488.
- Geissler, W. H., R. Kind, and X. H. Yuan (2008), Upper mantle and lithospheric heterogeneities in central and eastern Europe as observed by teleseismic receiver functions, *Geophys. J. Int.*, *174*, 351–376, doi:10.1111/j.1365-246X.2008.03767.x.
- Goes, S., W. Spakman, and H. Bijwaard (1999), A lower mantle source for central European volcanism, *Science*, *286*, 1928–1931, doi:10.1126/science.286.5446.1928.
- Harangi, S., H. Downes, M. Thirlwall, and K. Gméling (2007), Geochemistry, petrogenesis and geodynamic relationships of Miocene calc-alkaline volcanic rocks in the Western Carpathian Arc, eastern central Europe, *J. Petrol.*, *48*, 2261–2287, doi:10.1093/petrology/egm059.
- Hetényi, G., and Z. Bus (2007), Shear wave velocity and crustal thickness in the Pannonian Basin from receiver function inversions at four permanent stations in Hungary, *J. Seismol.*, *11*, 405–414, doi:10.1007/s10950-007-9060-4.
- Horváth, F. (1993), Towards a mechanical model for the formation of the Pannonian Basin, *Tectonophysics*, *226*, 333–357, doi:10.1016/0040-1951(93)90126-5.
- Horváth, F., and L. Royden (1981), Mechanism for the formation of the Intra-Carpathian Basins: A review, *Earth Evol. Sci.*, *3–4*, 307–316.
- Horváth, F., G. Bada, P. Szafián, G. Tari, A. Ádám, and S. Cloething (2005a), Formation and deformation of the Pannonian basin: Constraints from observational data, in *European Lithosphere Dynamics*, edited by D. Gee and R. Stephenson, *Geol. Soc. London Mem.*, *32*, 191–206.
- Horváth, F., *et al.* (2005b), Atlas of the present-day geodynamics of the Pannonian Basin: Euroconform maps with explanatory text, Eötvös Loránd Univ., Budapest. (Available at http://geophysics.elte.hu/projektek/geodinamikai_atlasz_eng.htm)
- Houseman, G. A., and L. Gemmer (2007), Intra-orogenic extension driven by gravitational instability: Carpathian-Pannonian orogeny, *Geology*, *35*, 1135–1138, doi:10.1130/G23993A.1.
- Kovács, I., L. Csontos, C. Szabó, E. Bali, G. Falus, K. Benedek, and Z. Zajacz (2007), Paleogene–early Miocene igneous rocks and geodynamics of the Alpine-Carpathian-Pannonian-Dinaric region: An integrated approach, in *Cenozoic Volcanism in the Mediterranean Area*, edited by L. Beccaluva *et al.*, *Geol. Soc. Am. Spec. Pap.*, *418*, 93–112.
- Langston, C. (1979), Structure under Mount Rainier, Washington, inferred from teleseismic body waves, *J. Geophys. Res.*, *84*, 4749–4762, doi:10.1029/JB084iB09p04749.
- Lawrence, J. F., and P. M. Shearer (2006), A global study of transition zone thickness using receiver functions, *J. Geophys. Res.*, *111*, B06307, doi:10.1029/2005JB003973.
- Lebedev, S., S. Chevrot, and R. D. van der Hilst (2002), Seismic evidence for olivine phase changes at the 410- and 660-kilometer discontinuities, *Science*, *296*, 1300–1302, doi:10.1126/science.1069407.
- Li, X. Q., and X. H. Yuan (2003), Receiver functions in northeast China—Implications for slab penetration into the lower mantle in northwest Pacific subduction zone, *Earth Planet. Sci. Lett.*, *216*, 679–691, doi:10.1016/S0012-821X(03)00555-7.
- Li, X., S. V. Sobolev, R. Kind, X. Yuan, and C. Estabrook (2000), A detailed receiver function image of the upper mantle discontinuities in the Japan subduction zone, *Earth Planet. Sci. Lett.*, *183*, 527–541, doi:10.1016/S0012-821X(00)00294-6.
- Lombardi, D., J. Braunmiller, E. Kissling, and D. Giardini (2009), Alpine mantle transition zone imaged by receiver functions, *Earth Planet. Sci. Lett.*, *278*, 163–174, doi:10.1016/j.epsl.2008.11.029.
- Lorinczi, P., and G. A. Houseman (2009), Lithospheric gravitational instability beneath the Southeast Carpathians, *Tectonophysics*, doi:10.1016/j.tecto.2008.05.024, in press.
- Ono, S. (2007), The Lehmann discontinuity due to dehydration of subducted sediment, *Open Mineral. J.*, *1*, 1–4.
- Piromallo, C., and A. Morelli (2003), *P* wave tomography of the mantle under the Alpine-Mediterranean area, *J. Geophys. Res.*, *108*(B2), 2065, doi:10.1029/2002JB001757.
- Piromallo, C., D. Gasperini, P. Macera, and C. Faccenna (2008), A late Cretaceous contamination episode of the European–Mediterranean mantle, *Earth Planet. Sci. Lett.*, *268*, 15–27, doi:10.1016/j.epsl.2007.12.019.
- Schmid, S. M., D. Bernouilli, B. Fügenschuh, L. Matenco, S. Schefer, R. Schuster, M. Tischler, and K. Ustaszewski (2008), The Alpine-Carpathian-Dinaric orogenic system: Correlation and evolution of tectonic units, *Swiss J. Geosci.*, *101*, 139–183, doi:10.1007/s00015-008-1247-3.

- Shearer, P. M., and G. Masters (1992), Global mapping of topography on the 660-km discontinuity, *Nature*, 355, 791–796, doi:10.1038/355791a0.
- Środa, P., W. Czuba, M. Grad, A. Guterch, A. K. Tokarski, T. Janik, M. Rauch, G. R. Keller, E. Hegedűs, J. Vozár, and the CELEBRATION 2000 Working Group (2006), Crustal and upper mantle structure of the Western Carpathians from CELEBRATION 2000 profiles CEL01 and CEL04: Seismic models and geological implications, *Geophys. J. Int.*, 167, 737–760, doi:10.1111/j.1365-246X.2006.03104.x.
- Stampfli, G. M., and G. D. Borel (2004), The TRANSMED transects in space and time: Constraints on the paleotectonic evolution of the Mediterranean domain, in *The TRANSMED Atlas: The Mediterranean Region from Crust to Mantle*, edited by W. Cavazza et al., pp. 53–80, Springer, Heidelberg, Germany.
- Świczak, M., M. Grad, and the TOR and SVEKALAPKO Working Groups (2004), Upper mantle seismic discontinuities topography variations beneath eastern Europe, *Acta Geophys. Pol.*, 52, 251–270.
- Wessel, P., and W. H. F. Smith (1991), Free software helps map and display data, *Eos Trans. AGU*, 72(41), 441, doi:10.1029/90EO00319.
- Wortel, M. J. T., and W. Spakman (2000), Subduction and slab detachment in the Mediterranean–Carpathian region, *Science*, 290, 1910–1917, doi:10.1126/science.290.5498.1910.
- Zhu, L. P. (2000), Crustal structure across the San Andreas Fault, southern California from teleseismic converted waves, *Earth Planet. Sci. Lett.*, 179, 183–190, doi:10.1016/S0012-821X(00)00101-1.
-
- E. Brückl, Institute of Geodesy and Geophysics, Technische Universität Wien, Gusshausstrasse 27-29, A-1040 Vienna, Austria.
- E. Hegedűs, Eötvös Loránd Geophysical Institute, Kolumbusz utca 17-23, H-1145 Budapest, Hungary.
- G. Hetényi, Department of Earth Sciences, ETH Zurich, CH-8092 Zürich, Switzerland. (gyorgy.hetenyi@erdw.ethz.ch)
- F. Horváth, Department of Geophysics, Eötvös University, Pázmány Péter sétány 1/C, H-1117 Budapest, Hungary.
- G. A. Houseman and G. W. Stuart, School of Earth and Environment, University of Leeds, Leeds LS2 9JT, UK.

Auxiliary Material for the manuscript:

Anomalously deep mantle transition zone below Central Europe: evidence of lithospheric instability

by G. Hetényi, G. W. Stuart, G. A. Houseman, F. Horváth, E. Hegedűs, and E. Brückl

1. Data and processing details

Figure 1 shows the broad-band seismological stations providing data for our study. The Carpathian Basins Project (CBP) [Houseman et al., 2008] deployed three profiles with an average sensor spacing of 30 km between April 2006 and August 2007 (CBP 6TD, Fig. 1), together with a regional network of 10 sensors (CBP 3T, Fig. 1), which operated for two years from September 2005. We also included data from permanent stations from the end of 2003 (the beginning of recording of most of these stations) to the end of 2007. All traces originating from teleseismic earthquakes ($m_b \geq 5.7$ for the CBP data; $m_b \geq 6.0$ for the permanent stations) with epicentral distances between 30 and 90 degrees were initially analyzed; a later automatic quality control stage weeded out poor signals. The 101 stations produced 15,099 three-component records suitable for receiver function computation. The corresponding piercing points at the 410 and the 660 km discontinuities ('410' and '660' hereinafter) are shown on Figure S1. This distribution provides the resolution for performing 3-D imaging, especially when taking into account the width of the Fresnel zone at mantle transition zone (MTZ) depths. (The Fresnel zone has a ~ 125 and ~ 160 km radius, respectively at the '410' and the '660', at the higher corner frequency of 0.25 Hz).

We applied the time-domain iterative deconvolution technique [Ligorria and Ammon, 1999] to compute receiver functions, using a large number of spikes (equivalent to 20% of the total trace length) in order to allow the recovery of broad peaks corresponding to potential velocity gradients. Initially the traces were band-pass filtered between 0.033 to 0.25 Hz; after deconvolution the resulting spike series were convolved with a Gaussian filter of 4 seconds width. RFs with low signal-to-noise ratio, atypical ringing waveforms or abnormal amplitudes were removed during a

final quality control procedure, which resulted in 5773 traces used in the final 3-D image. The back-azimuthal distribution of both the original and the selected dataset are shown on Figure S2.

Migration of the RFs was performed using the common conversion point technique [Zhu, 2000]. The S-wave model has been calculated from the PM05 regional P-wave velocity-model [Piromallo and Morelli, 2003] assuming the same depth-dependence of V_p/V_s as the global *iasp91* model [Kennett and Engdahl, 1991]. The influence of using a 3-D vs. a 1-D velocity model for migration was assessed by comparison of two images: together with similar shapes obtained, there were local differences in migrated depths of 3-4 km maximum. Prior to migration, we apply a time correction to account for delays caused by variable thickness of the sedimentary cover, using the Pre-Tertiary basement contour map of Kilényi and Šefara [1989] and velocities from Šroda *et al.* [2006] together with a V_p/V_s ratio of 2.0. The individual RFs were migrated along their respective raypath, their amplitude binned into $20 \text{ km} \times 20 \text{ km} \times 4 \text{ km}$ size voxels and then averaged. The vertical size of the bins is slightly smaller than the potential vertical resolution of RFs at the considered frequencies and depths ($\sim 4.8\text{-}5$ and $\sim 5.5\text{-}6$ km at the ‘410’ and ‘660’, respectively). Finally, to take into account the size of the Fresnel zone, the image was smoothed with a Gaussian of $\sigma = 2$ voxels and cutting to zero beyond 7 (1) neighboring horizontal (vertical) voxels (i.e. over 140 and 4 km, respectively). Thus we produced our final 3-D migrated receiver function image beneath the Pannonian Basin region.

Multiply reflected phase conversions, particularly from crustal interfaces, can complicate the interpretation of receiver functions. On investigation we conclude that all crustal multiples arrive at times corresponding to depths less than 200 km. In theory a surface multiple from the ephemeral Lehmann discontinuity (~ 220 km depth) could arrive at an apparent depth near the bottom of the transition zone. However, there is little evidence for this discontinuity in our region of study.

2. Thickening of the MTZ: the effect of V_p/V_s and waveforms

The observation of a flat ‘410’ and an undulating ‘660’ by migrated receiver functions raises the question whether the application of a laterally homogeneous V_p/V_s within the MTZ is correct, and whether the observed undulations are real or not. To our knowledge, there is no seismological approach that allows determination of V_p/V_s within the MTZ, but it is possible to calculate the required increase in V_p/V_s that would delay converted waves equivalent to ~ 40 km in depth. These calculations show that this necessary increase is more than 10%, meaning that the entire MTZ has a V_p/V_s exceeding 2.00-2.05. This is only realistic if significant amount of melt is present, which is one possible scenario according to large-scale tomography images (Goes et al., 1999). However, in order to explain the ~ 40 km amplitude undulations of the ‘660’, the V_p/V_s -ratio should present significant lateral variations on relatively short wavelengths, which is not plausible with the idea of a widespread plume. Beyond these calculations, there are other means to visualize the thickening of the MTZ that are devoid of time-to-depth conversion artifacts.

To support lateral variations in MTZ thickening free from migration artifacts, we determine the relative delay time between the ‘410’ and ‘660’ peaks for three geographically distinct areas (see Figure 1 for locations): the Western Carpathians (A), the eastern Pannonian Basin (B), and the southern edge of the Bohemian Massif near the Vienna Basin (C) (see Figs. 1 and S1 for location). To do so, we have produced time-domain stacks of the receiver function waveforms which have their ‘410’ or ‘660’ piercing-points within a 140 km radius circle (corresponding to an average Fresnel zone) of the three locations. Individual traces were summed according to a weighting inversely proportional to distance, by using a Gaussian located at the respective centers. The six respective move-out corrected stacks are shown on Figure S3, with vertical lines showing the expected delay times based on *iasp91* [Kennett and Engdahl, 1991]. For the ‘410’, zones B and C exhibit normal arrival times, and zone A has a delay of about 2 seconds. For the ‘660’, the peaks are slightly broader and occur up to 6 seconds late, corresponding to the depth range observed on the

migrated images. Zone *B*, with ~6 seconds delay, samples the bowl-shaped depression mentioned in the main text and shown on Figure 2. In conclusion, the time-domain stacks confirm the perception from the migrated images: a ‘410’ with regular delay times and only minor variations in depth, and a ‘660’ with delayed/deepened peaks and significant topography.

3. Resolution and intermittency of MTZ discontinuities

Figure 2 reveals not only the structure of the MTZ, but also another interesting observation, namely that both the ‘410’ and the ‘660’ appear as intermittent discontinuities. This is partly related to ray-coverage issues and the variable quality of the data, which we believe is the dominant factor for the ‘660’. In the meantime, in the case of the ‘410’, amplitude variations exist in zones of similar ray density and may contain information about lateral variability of this velocity discontinuity. These variations might be related to water content. Increasing water content broadens the depth range across which the olivine-to-wadsleyite phase change (and hence velocity increase) takes place (Frost and Dolejs, 2006), and such a velocity-gradient will produce broader RF peaks with lower amplitudes.

References

- Frost, D. J., and D. Dolejs, D. (2006), Experimental determination of the effect of H₂O on the 410-km seismic discontinuity, *Earth Planet. Sci. Lett.*, 256, 182–195, doi:10.1016/j.epsl.2007.01.023
- Goes, S., W. Spakman, and H. Bijwaard (1999), A lower mantle source for central European volcanism, *Science*, 286, 1928–1931.
- Houseman, G., G. Stuart, E. Hegedűs, E. Brückl, S. Radovanovic, A. Brisbane, P. Lorinczi, B. Dando, A. Kovács, and H. Hausmann (2008), Preliminary results from the Carpathian Basins

Project: an investigation of the seismic structure of the lithosphere in the Pannonian and Vienna Basins, *Geophys. Res. Abs.*, 10, EGU2008-A-05716.

Kennett, B. L. N., and E. R. Engdahl (1991), Traveltimes for global earthquake location and phase identification, *Geophys. J. Int.*, 105, 429–465.

Kilényi, E., and J. Šefara (Eds.) (1989), *Pre-Tertiary basement contour map of the Carpathian Basin beneath Austria, Czechoslovakia and Hungary, Map 1:500'000*, ELGI, Budapest.

Ligorria, J., and C. J. Ammon (1999), Iterative deconvolution and receiver-function estimation, *Bull. Seismol. Soc. Am.*, 89, 1395–1400.

Piomallo, C., and A. Morelli (2003), P wave tomography of the mantle under the Alpine-Mediterranean area, *J. Geophys. Res.*, 108, 2065, doi:10.1029/2002JB001757

Šroda, P., W. Czuba, M. Grad, A. Guterch, A. K. Tokarski, T. Janik, M. Rauch, G. R. Keller, E. Hegedűs, J. Vozár, and the CELEBRATION 2000 Working Group (2006), Crustal and upper mantle structure of the Western Carpathians from CELEBRATION 2000 profiles CEL01 and CEL04: seismic models and geological implications, *Geophys. J. Int.*, 167, 737–760.

Tauzin, B., E. Debayle, and G. Wittlinger (2008), The mantle transition zone as seen by global Pds phases: No clear evidence for a thin transition zone beneath hotspots, *J. Geophys. Res.*, 113, B08309, doi:10.1029/2007JB005364

Zhu, L. P. (2000), Crustal structure across the San Andreas Fault, southern California from teleseismic converted waves, *Earth Planet. Sci. Lett.*, 179, 183–190.

Figure captions

Figure S1

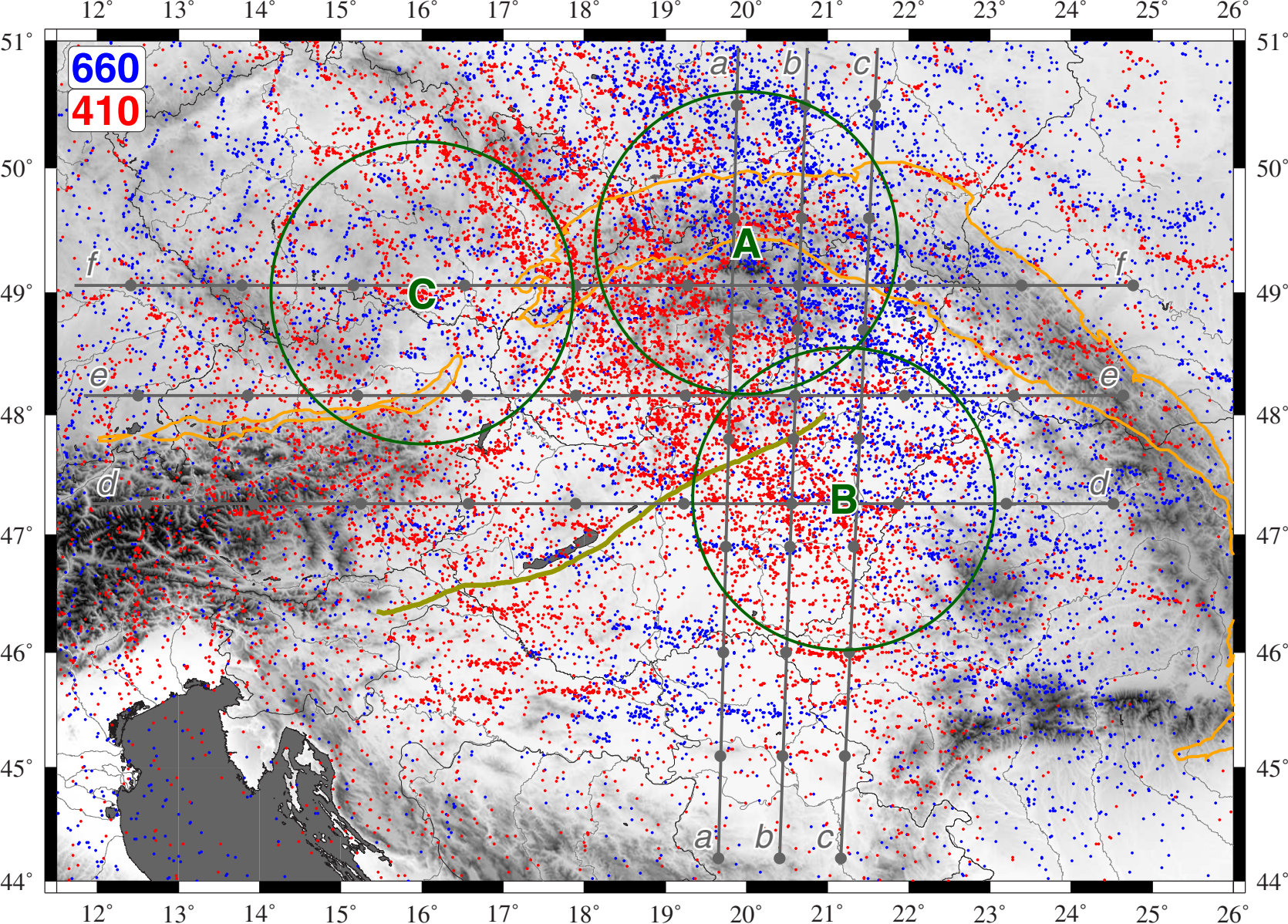
Piercing points of the teleseismic rays at the 410 km (red) and the 660 km (blue) discontinuity determined from the *iasp91* velocity model [Kennett and Engdahl, 1991]. Migrated profiles *a-f* are presented on Fig. 2a-f. Circles A-C are 140 km radii areas for waveform stacking shown on Fig. S3. The Mid-Hungarian Line and the Carpathian flysch are drawn for reference. Dots on profiles are at 100 km intervals.

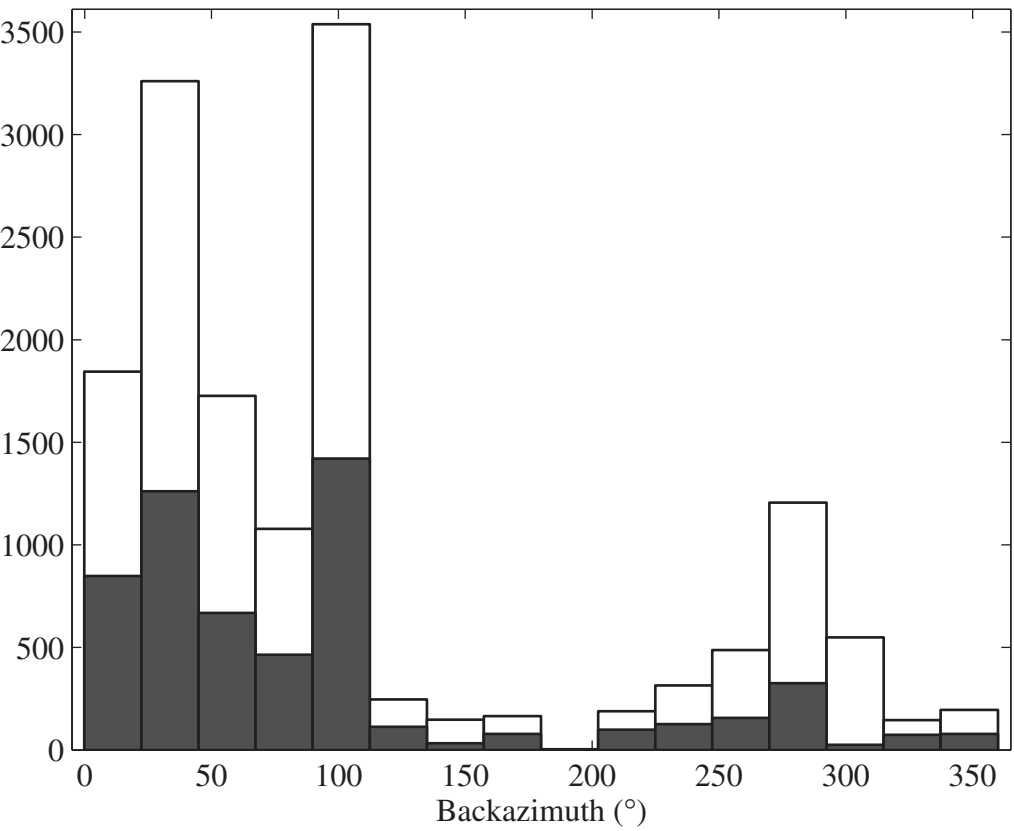
Figure S2

Azimuthal coverage of the receiver function dataset showing that the majority of the signal arrives from East and Northeast. The histogram in white shows the distribution of event-station couples for the entire dataset (15,099 traces), while the histogram in grey corresponds to the dataset after quality control (5773 traces).

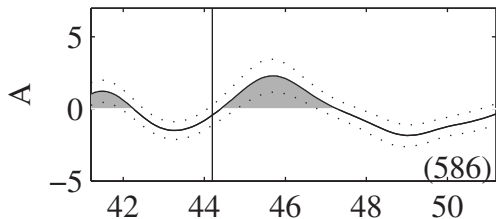
Figure S3

Receiver function stacks in three circular regions (see Figs. 1 and S1) around the 410 km (left) and the 660 km (right) discontinuities. The vertical lines at 44.2 and 68.2 s, respectively, mark the theoretical delay time from ray tracing for a surface event at 65° epicentral distance [Tauzin et al., 2008] using the *iasp91* velocity model [Kennett and Engdahl, 1991]. The traces were move-out corrected and weighted inversely proportional to distance; their number in each stack is shown in parentheses. The vertical axis is multiplied by 1000. Errors were evaluated by bootstrapping: the two dotted lines show the waveforms at 5% and 95% of 10,000 randomly selected and sorted stacks.

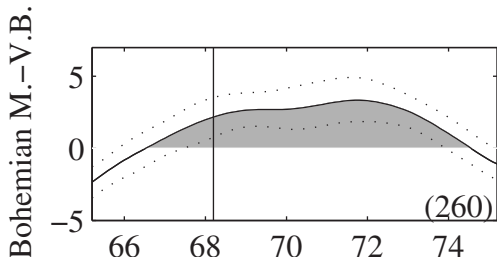
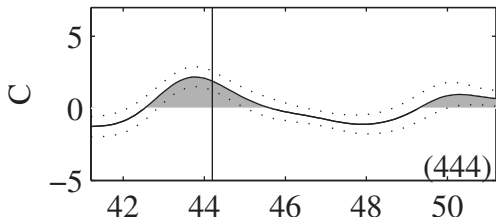
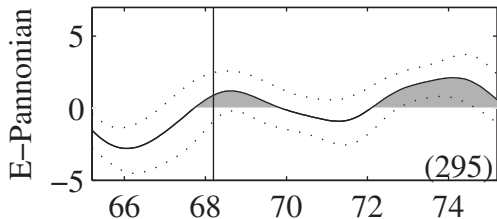
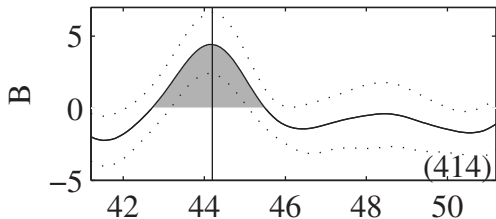
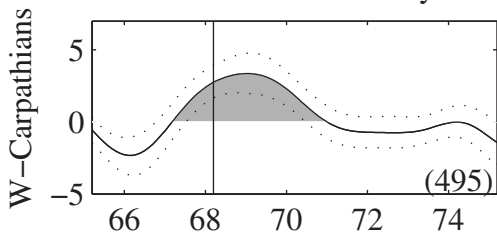




410-km discontinuity



660-km discontinuity



Time after P-wave arrival (sec)

Time after P-wave arrival (sec)